Published in final edited form as:
Cell Calcium. 2009 March ; 45(3): 310–317. doi:10.1016/j.ceca.2008.11.003.

2-Aminoethoxydiphenyl-borate (2-APB) increases excitability in pyramidal neurons

Anna M. Hagenston[a,*], **Noam D. Rudnick**[a], **Christine E. Boone**[a], and **Mark F. Yeckel**[a,b]

[a]Department of Neurobiology, Yale University School of Medicine, Germany

[b]The Kavli Institute for Neuroscience, Yale University School of Medicine, Germany

Abstract

Calcium ions (Ca^{2+}) released from inositol trisphosphate (IP_3)-sensitive intracellular stores may participate in both the transient and extended regulation of neuronal excitability in neocortical and hippocampal pyramidal neurons. IP_3 receptor (IP_3R) antagonists represent an important tool for dissociating these consequences of IP_3 generation and IP_3R-dependent internal Ca^{2+} release from the effects of other, concurrently stimulated second messenger signaling cascades and Ca^{2+} sources. In this study, we have described the actions of the IP_3R and store-operated Ca^{2+} channel antagonist, 2-aminoethoxydiphenyl-borate (2-APB), on internal Ca^{2+} release and plasma membrane excitability in neocortical and hippocampal pyramidal neurons. Specifically, we found that a dose of 2-APB (100 μM) sufficient for attenuating or blocking IP_3-mediated internal Ca^{2+} release also raised pyramidal neuron excitability. The 2-APB-dependent increase in excitability reversed upon washout and was characterized by an increase in input resistance, a decrease in the delay to action potential onset, an increase in the width of action potentials, a decrease in the magnitude of afterhyperpolarizations (AHPs), and an increase in the magnitude of post-spike afterdepolarizations (ADPs). From these observations, we conclude that 2-APB potently and reversibly increases neuronal excitability, likely via the inhibition of voltage- and Ca^{2+}-dependent potassium (K^+) conductances.

Keywords

Potassium channels; Pharmacology; IP_3 receptor; Internal calcium release

1. Introduction

An important determinant of neuronal activity is the intracellular concentration of calcium ions ($[Ca^{2+}]_i$). Changes in $[Ca^{2+}]_i$ are mediated by entry through voltage-gated Ca^{2+} channels (VGCCs) and ligand-gated channels (e.g., NMDA receptors), and by release of Ca^{2+} from intracellular stores such as the endoplasmic reticulum. There are two major classes of intracellular Ca^{2+} release channels in neurons, ryanodine receptor channels and IP_3Rs [1]. Ryanodine receptors are stimulated by cytosolic Ca^{2+}, while IP_3Rs are sensitive both to IP_3 and to Ca^{2+}. The dependence of IP_3Rs on both IP_3 and Ca^{2+} endows these receptors with the ability to respond differentially to a broad range of stimulus combinations and intensities [2, 3]. For example, stimuli that mobilize threshold levels of IP_3 may nonetheless evoke robust internal Ca^{2+} release when accompanied by a VGCC-mediated rise in $[Ca^{2+}]_i$ [4–6]. This characteristic of IP_3Rs complicates interpretation of the consequences of IP_3-mobilizing

*Corresponding author at: Institut für Neurobiologie, Im Neuenheimer Feld 364, Ruprecht-Karls Universität Heidelberg, D-69120 Heidelberg, Germany. Tel.: +49 6221 54 8355; fax: +49 6221 54 6700. hagenston@nbio.uni-heidelberg.de (A.M. Hagenston).

stimuli, as it suggests that IP_3R-mediated $[Ca^{2+}]_i$ rises and $[Ca^{2+}]_i$ rises dependent on the activation of VGCCs or NMDA receptors are not necessarily mutually exclusive.

IP_3 in neurons is generated following activation of $g_{q/11}$-coupled GTP-binding protein-coupled seven transmembrane domain receptors (GPCRs) such as group I metabotropic glutamate receptors (mGluRs) and M1-type muscarinic acetylcholine receptors (mAChRs) or $g_{i/o}$-coupled GPCRs such as M2-type mAChRs and α_2 adrenergic receptors. Following activation, these receptors stimulate g-protein guanine exchange and dissociation into g_α and $g_{\beta\gamma}$ subunits. $G_{q/11\alpha}$ and $g_{i/o\beta\gamma}$ subunits, in turn, stimulate phospholipase C in the plasma membrane, which cleaves the membrane phospholipid phosphatidylinositol bis-phosphate into IP_3 and diacylglycerol (DAG). Mobilized IP_3 diffuses through the cytosol to bind IP_3Rs, while DAG binds to and activates protein kinase C. Disentangling the particular effects of IP_3 mobilization and subsequent IP_3R activation downstream from GPCR stimulation is thus further complicated by the fact that the events leading to IP_3 production also generate at least two additional second messengers, $g_{q/11\beta\gamma}$ or $g_{i/o\alpha}$ and DAG.

IP_3R activation in neocortical and hippocampal pyramidal neurons triggers propagating waves of internally released Ca^{2+} [7–11]. Two particularly intriguing consequences of these Ca^{2+} waves are the activation of a transient SK-type Ca^{2+}-dependent K^+ channel-mediated membrane hyperpolarization and the generation of a prolonged membrane depolarization (e.g., Fig. 1A and B; [11–15]). *In vitro*, these changes in membrane potential have been observed to alter the excitability and spiking patterns of individual pyramidal neurons [11–14]. Whether IP_3R-mediated Ca^{2+} waves can similarly alter neuronal excitability *in vivo*, and how IP_3R-dependent excitability changes might influence patterns of network activity and, ultimately, animal behavior are important questions. The importance of understanding how IP_3R-dependent Ca^{2+} signaling contributes to normal cognitive function is underlined by a recent series of studies implicating dysregulated internal Ca^{2+} release in the pathophysiology of Alzheimer's disease [16–19]. The results of these studies furthermore raise the question of whether IP_3Rs might represent an important therapeutic target for the treatment of cognitive dysfunction. Our ability to address these and other questions whose aim it is to identify and understand the particular consequences of IP_3R-dependent internal Ca^{2+} release is naturally limited by the selection of available experimental tools. One of the most valuable of these tools is a pharmacological IP_3R antagonist. Ideally, any pharmacological agent employed in the study of IP_3R signaling would be potent, specific, and membrane-permeant.

There are two commonly employed classes of commercially available and membrane-permeant IP_3R antagonists: the marine sponge toxin xestospongin C and the boron compound 2-APB. Neither of these pharmacological agents acts only on IP_3Rs, however. Xestospongin C, while a potent IP_3R antagonist in some preparations [20,21], has in other preparations failed entirely to inhibit IP_3R-mediated internal Ca^{2+} release [22,23]. Furthermore, it has been suggested to antagonize store-operated Ca^{2+} channels (SOCs) [24], and to interfere with Ca^{2+} store loading via antagonism of sarco-endoplasmic reticulum Ca^{2+} (SERCA) pumps [20,22,25, but see 26]. Xestospongin C has also been reported to inhibit voltage-dependent Ca^{2+} and K^+ currents in smooth muscle cells, although this finding has not been verified in neuronal preparations [23]. 2-APB has a similar and similarly large repertoire of targets, including IP_3Rs [27–30, but see 22], SOCs [27–29,31], SERCA pumps [27–29,32], and transient receptor potential channels [33–35]. Furthermore, 2-APB has been shown to inhibit voltage-gated K^+ channels [36], and is suggested to interfere with Ca^{2+} signaling mediated by voltage-gated Ca^{2+} channels [29].

Here we describe our observations that 2-APB consistently inhibits, but inconsistently blocks IP_3-evoked internal Ca^{2+} release and Ca^{2+} waves and that 2-APB increases neuronal excitability in neocortical and hippocampal pyramidal neurons. Based on these findings, we

conclude that 2-APB is of limited utility for studies seeking to examine how IP_3R-mediated Ca^{2+} signaling and subsequent alterations in neuronal excitability might influence activity patterns in individual neurons, neuronal networks and systems, and, ultimately, animal behavior.

2. Materials and methods

2.1. Slice preparation

Brain slices were prepared from P22–P35 male Sprague–Dawley rats (n = 19 animals) as previously described [11]. Briefly, animals were anesthetized with a mixture of ketamine, xylazine, and acepromazine, and decapitated when no longer responsive to a foot pinch. Coronal slices of the medial prefrontal cortex (320 μm) and horizontal hippocampal slices (350 μm) were cut using a Vibratome in a peltier-cooled slicing chamber filled with dissecting solution and maintained at a temperature between 0.5 and 3.0 °C. The dissection solution was continuously bubbled with 95% O_2/5% CO_2, and contained (in mM): 87 NaCl, 75 sucrose, 10 dextrose, 2.5 KCl, 25 $NaHCO_3$, 1.3 NaH_2PO_4, 7.0 $MgCl_2$, 0.5 $CaCl_2$, adjusted with sucrose to 295–305 mOsm. After cutting, the brain slices were incubated for 10–20 min in 34–37 °C dissecting solution, and then transferred to 34–37 °C recording artificial cerebrospinal fluid (ACSF) and allowed to cool to room temperature for at least 1 h prior to recording. Standard recording ACSF contained (in mM): 124 NaCl, 10 dextrose, 2.5 $NaHCO_3$, 1.3 NaH_2PO_4, 2.0 $MgCl_2$, and 2.0 $CaCl_2$, adjusted with sucrose to 295–305 mOsm.

2.2. Whole-cell recordings and solutions

Individual slices selected for recordings were continuously perfused with 95% O_2/5% CO_2-saturated recording ACSF (flow rate 1–2 ml/min) and maintained at 31–34 °C throughout the course of each experiment. Visualized whole-cell patch clamp recordings were performed using infrared differential interference contrast (DIC) microscopy on an upright microscope (Zeiss Axioskop or Olympus BX51WI) with thick-walled borosilicate glass patch pipettes (2–5MΩ). The pipette solution contained (in mM): 134 $KMeOSO_3$, 10 HEPES, 3.0 KCl, 1.0 $MgCl_2$, 4.0 Mg-ATP, 0.5 Na-GTP, 5.0K_2-phosphocreatine, 5.0 Na_2-phosphocreatine, pH adjusted with KOH to 7.52–7.55, 285–290 mOsm, as well as 50 units/ml creatine phosphokinase, 5–15 μM Alexa 488 or Alexa 568 for visualization of filled processes under fluorescent illumination, and one of the following Ca^{2+} indicator dyes: 100 μM bis-fura-2, 200 μM fura-2ff, 100 μM fluo-4, or 100 μM Oregon Green 488 BAPTA-2. $KMeOSO_3$, Mg-ATP, Na-GTP, Na_2-phosphocreatine, and creatine phosphokinase were obtained from Sigma–Aldrich (St. Louis, MO). K_2-phosphocreatine was obtained from Calbiochem (San Diego, CA). Alexa 488, Alexa 568, bis-fura-2, fluo-4, and Oregon Green 488 BAPTA-2 were purchased from Molecular Probes/Invitrogen (Carlsbad, CA). For uncaging experiments, the internal solution was supplemented with 97 μM NPE-caged IP_3 (Calbiochem/EMD Biosciences; San Diego, CA). Electrical signals were acquired at 2 kHz using an SEC 05LX amplifier (npi electronic; Tamm, Germany) in bridge or discontinuous voltage-clamp mode, digitized, and analyzed on- and off-line using custom software developed in IGOR Pro (WaveMetrics; Portland, OR). Whole-cell series resistance ranged from 5 to 37 MΩ and was compensated for by adjusting the bridge balance. Data were not corrected for junction potential (~10 mV). Cells were held at approximately −65 mV (prefrontal cortical neurons) or −63 mV (CA1 hippocampal pyramidal neurons) for the duration of the experiment. The 26 prefrontal cortical and three CA1 hippocampal pyramidal neurons included in this study had an average resting membrane potential of −59.1 ± 0.9 mV (cells were discarded if > −50 mV), an average input resistance of 84.6 ± 5.2 MΩ, and exhibited spike frequency adaptation in response to prolonged (300 ms) suprathreshold current injection. 2-APB (100 μM; Tocris Bioscience; Ellisville, MO) was prepared as a 100 mM stock solution in DMSO.

2.3. Ca^{2+} fluorescence imaging

Ca^{2+} indicator dye diffused into the recorded neuron via the patch pipette. Dye fluorescence was imaged using a cooled CCD camera (Quantix 57 or Cascade 512B; Photometrics; Tucson, AZ). Images were collected at 50 or 25 Hz with 2 × 2 to 5 × 5 pixel binning. Epifluorescence illumination was provided by a 150 W short-arc xenon bulb (Optiquip; Highland Mills, NY). Relative changes in $[Ca^{2+}]_i$ were quantified as changes in $\Delta F/F = |F(t) - F|/F$, where F represents baseline fluorescence intensity prior to stimulation and ΔF represents the magnitude of fluorescence change during activity. Optical data were corrected for tissue autofluorescence and smoothed with 5- to 10-frame averaging. Relative changes in dye fluorescence in regions of interest over the soma and dendrites are displayed as changes in the amplitude of correspondingly colored optical traces.

2.4. Stimulation

Synaptic afferents were electrically stimulated using a glass microelectrode (5–10 μm tip diameter) with a fine tungsten rod glued to its side and filled with standard recording ACSF. Stimulating electrodes were placed ~20–60 μm away from the recorded cell body and ~20–50 μm to one side of its primary apical dendrite. Trains of unipolar pulses (20–50 stimuli, 15–150 μA, 0.1 ms, 50–100 Hz,) were delivered to elicit internal Ca^{2+} release. For focal pharmacological mGluR stimulation, a 2–5 MΩ pipette was filled with the group I/II mGluR agonist (±)-1-aminocyclopentanetrans-1,3-dicarboxylic acid (ACPD, 400 μM; Tocris Bioscience) in standard recording solution or in recording solution where 10 mM HEPES replaced 10 mM dextrose, and positioned ~20–60 μm away from the soma and <10 μm to one side of the primary apical dendrite. Focal stimulation of ryanodine receptors was similarly accomplished using a 2–5 MΩ pipette filled with caffeine (50 mM; Sigma–Aldrich) in standard recording solution and placed adjacent to the primary apical dendrite. NPE-caged IP_3 diffused into the recorded neuron via the patch pipette. Photolysis of NPE-caged IP_3 was achieved with 50–500 ms flashes of UV light (320–400 nm) produced by a 100 W mercury lamp (HBO ebq 100 isolated; Carl Zeiss, Inc.; Thornwood, NY). The photolysis beam (~20 μm diameter) was directed onto the soma or proximal apical dendrite of the recorded cell using a custom-made fiber optic spot illumination system (Rapp OptoElectronic GmbH; Hamburg, Germany) fitted to the aperture stop port in the epi-illumination pathway of an Olympus BX51WI microscope.

2.5. Data analysis

Input resistance was calculated from the average voltage response to a train of hyperpolarizing current pulses (150–250 pA, 300 ms duration). Voltage responses were measured during the last 20 ms of each 300 ms square pulse current injection and compared to baseline membrane potential in the 20 ms prior to current injection. Action potential heights were measured from the average membrane potential 20 ms prior to action potential onset and to the peak of the membrane potential deflection. Action potential widths were calculated at half-maximum amplitude. Single spike ADPs were calculated as the difference between the average membrane potential in the 5–20 ms following the onset of the action potential and the average membrane potential in the 20 ms prior to action potential onset. Single spike AHPs were calculated as the difference between the minimum membrane potential >1 ms following the peak of the action potential and the average membrane potential in the 2–7 ms prior to action potential onset. The time at which an action potential occurred was defined as the time at which the somatically recorded membrane potential reached its peak. *Control*, *drug*, and *wash* conditions typically corresponded to the following time periods: 15–0 min prior to 2-APB application, 10–30 min following addition of 2-APB to the recording ACSF, and 15–30 min after the start of 2-APB wash-out. Data from control cells were analyzed such that "*control*" and "*drug*" time periods were defined as 0–15 min and 30–45 min following the experimenter's initial assessment of cellular health and/or internal Ca^{2+} release potential.

2.6. Statistics

As there were no obvious differences in responses across ages or cell types, data were pooled. Data are presented as mean ± S.E.M. Statistical significance ($p < 0.05$) was assessed using two-tailed unpaired Student's *t*-tests.

3. Results and discussion

3.1. 2-APB inhibits internal Ca^{2+} release

We first examined the effects of 2-APB on IP_3R-dependent internal Ca^{2+} release and Ca^{2+} waves in neocortical and hippocampal pyramidal neurons in an *in vitro* slice preparation. Three different stimulation techniques were used to trigger internal Ca^{2+} release: focal pharmacological stimulation of mGluRs with the group I/II mGluR agonist ACPD (*ACPD puffing*), focal photolysis of NPE-caged IP_3 (*IP_3 uncaging*), and electrical stimulation of synaptic afferents. Regardless of the technique employed, we observed that 100 μM 2-APB consistently inhibited internal Ca^{2+} release, typically within less than 15 min ($n = 15/17$; inhibition first observed after 11.7 ± 1.3 min 2-APB exposure). More specifically, we found that 2-APB attenuated the amplitude and extent of Ca^{2+} waves in 4/9 neurons stimulated with puffs of ACPD (Fig. 1A), in 2/3 neurons where release was evoked by IP_3 uncaging (Fig. 1B), and in 3/5 synaptically stimulated neurons. In one cell stimulated with puffs of ACPD and in another cell stimulated with uncaged IP_3, 2-APB had no apparent effect on internal Ca^{2+} release (data not shown). 2-APB blocked internal Ca^{2+} release and Ca^{2+} waves in each of the remaining neurons tested ($n = 6/17$; block first observed after 11.3 ± 2.9 min 2-APB exposure; Fig. 1C). We did not observe recovery of internal Ca^{2+} release during 2-APB wash-out ($n = 2$). These findings are consistent with reports suggesting that 2-APB inhibits internal Ca^{2+} release by antagonizing IP_3Rs, and are also in agreement with the observation that 2-APB only inconsistently blocks internal Ca^{2+} release evoked by IP_3R stimulation [27]. Importantly, the inhibition by 2-APB of IP_3-induced internal Ca^{2+} release depends on the relative concentrations of 2-APB and IP_3 [28]. Our observation that 2-APB failed to block Ca^{2+} waves in over half of all cells stimulated synaptically or with puffs of ACPD ($n = 8/14$; release still present after 22.4 ± 2.7 min 2-APB exposure) and in every cell for which internal release was triggered by IP_3 uncaging ($n = 3/3$; release still present after 30.3 ± 0.9 min 2-APB exposure) may therefore suggest that, in some cells, 2-APB is being out-competed by IP_3.

Previous reports have suggested that, in addition to antagonizing IP_3Rs, 2-APB may also influence intracellular Ca^{2+} signaling via inhibition of SERCA pumps [27–29,32]. Given the dependence of internal Ca^{2+} release in pyramidal neurons on prior VGCC-mediated Ca^{2+} influx and presumed loading of the readily releasable intracellular Ca^{2+} pool [11,37,38], it seems possible that the inhibition by 2-APB of IP_3R-mediated internal Ca^{2+} release may result from 2-APB-dependent SERCA pump antagonism and consequent slow depletion of intracellular Ca^{2+} stores [27–29,32]. To further explore this possibility, we tested whether 2-APB inhibited internal Ca^{2+} release triggered by focal pressure application of the ryanodine receptor agonist, caffeine (*caffeine puffing*). We observed a reduction in the amplitude of caffeine-triggered internal Ca^{2+} release following 2-APB exposure ($n = 3/3$; inhibition first observed after 23.3 ± 1.9 min 2-APB exposure; Fig. 1D). However, the duration of 2-APB exposure prior to this inhibition was significantly greater than the duration of 2-APB exposure prior to inhibition or block of IP_3R-mediated internal Ca^{2+} release ($p < 0.0001$ for both measures). Moreover, 2-APB did not completely block Ca^{2+} waves evoked by caffeine puffing in any of the cells tested ($n = 3/3$; release still present after 33.3 ± 1.3 min 2-APB exposure). While 2-APB-mediated SERCA pump antagonism may contribute to the inhibition of internal Ca^{2+} release in pyramidal neurons, it seems unlikely that this effect could, on its own, account for the inhibition by 2-APB of IP_3R-mediated internal Ca^{2+} release.

3.2. 2-APB increases neuronal excitability

In addition to its effects on internal Ca^{2+} release, we also observed that 2-APB elevated pyramidal neuron excitability. This increased excitability was readily identified as a change in the characteristics of action potential waveforms and spike trains. We examined action potentials evoked by prolonged (300 ms) and brief (2 ms) suprathreshold current injections. Action potential trains evoked by prolonged current injection under control conditions initiated after a slight delay (delay to 1st spike, 46.8 ± 1.4 ms, $n = 12$) and exhibited spike frequency adaptation (Fig. 2A). Subsequent to 2-APB application, delays preceding the onset of action potential trains were reduced. A comparison of averaged measurements made during the control period (in the 15 min prior to 2-APB application) and the drug period (between 10 and 30 min following 2-APB application) revealed that this change was significant. In particular, we observed that the delay to 1st recorded action potential was 29.8 ± 3.6 ms sooner in the presence of 2-APB than it was under control conditions ($n = 12$; $p < 0.001$; Fig. 2A and D). Spike frequency adaptation was also inhibited following 2-APB application. This inhibition was apparent as an elevation in the rate of action potential generation immediately following the first action potential (Fig. 2A and D), and was quantified using the firing frequency in the first 100 ms of a spike train. This firing frequency was significantly greater in the presence of 2-APB than during the control period (13.4 ± 3.8 Hz faster, $n = 11$; $p < 0.05$). In pyramidal neurons, both the delay preceding the onset of the first action potential in a spike train evoked by prolonged square pulse current injection and the frequency of action potentials at the start of the spike train are regulated by voltage-gated K^+ currents [39,40]. The changes we observed in both these quantities therefore suggest that 2-APB may inhibit voltage-dependent K^+ conductances. This hypothesis is further supported by our observation that action potentials triggered by both prolonged and brief current injection were significantly broader in the presence of 2-APB than action potentials evoked under control conditions (Figs. 2A, B, E and 3C, E). The mean width of the 4th action potential triggered by prolonged current injection, for example, was 0.67 ± 0.09 ms greater in the 10–30 min after 2-APB application than it was in the control period ($n = 10$; $p < 0.001$). Increases in action potential width did not result from a change in the kinetics of the action potential upstroke, as one might expect if Na^+ conductances were affected, but rather from attenuation in the rate of membrane repolarization (Fig. 2A). Action potential repolarization in pyramidal neurons is controlled by voltage-dependent K^+ conductances distinct from those involved in setting the delay to action potential initiation or the rate of firing during a spike train [39–42]. Based on this observation, we find it highly likely that 2-APB inhibits multiple families of voltage-dependent K^+ conductances, including rapidly activating delayed-rectifier K^+ channels of the K_V class and slowly gated delayed-rectifier K^+ channels of the KCNQ class. This result is in agreement with a report indicating that 2-APB inhibits two voltage-dependent K^+ currents with very different kinetics in *Limulus* photoreceptors [36].

Afterhyperpolarizations were also significantly diminished in the 10–30 min following addition of 2-APB to the recording ACSF (Fig. 2A, C and F). The mean AHP of the 4th action potential triggered by prolonged current injection, for example, was 6.3 ± 0.8 mV smaller during 2-APB exposure than it was under control conditions ($n = 7$, $p < 0.001$). AHPs in pyramidal neurons are mediated predominantly by Ca^{2+}-dependent K^+ conductances [39–41, 43,44]. Indeed, the reduction in firing frequency observed over the course of a prolonged suprathreshold current injection is thought to depend strongly on the accumulation of Ca^{2+} entering the neuron via VGCCs and subsequent activation of SK-type and other Ca^{2+}-dependent K^+ channels [39,40,43]. Antagonism of Ca^{2+}-dependent K^+ conductances therefore results in diminished AHPs and reduced late phase spike frequency adaptation. Inhibition by 2-APB of SK or other Ca^{2+}-dependent K^+ channels might thus account for the observed decrease in AHP magnitudes as well as a part of the increase in firing rates of action potentials triggered by prolonged current injection.

In addition to AHPs, neocortical and hippocampal pyramidal neurons frequently exhibit an afterdepolarization that appears as a small hump at the base of an action potential trace (Fig. 3A; [39,45,46]). We examined the magnitudes of ADPs following action potentials evoked with 2 ms current injections, and found that they were significantly greater following 10–30 min bath application of 2-APB than they were in the 15 min prior to 2-APB exposure (8.8 ± 1.9 mV greater, $n = 14$; $p < 0.05$; Fig. 3A, B and D). The magnitude of ADPs depends, in part, on the amplitude of AHPs, such that antagonism of K^+ channels readily augments the ADP [45–47]. Our observation of an enhanced ADP is thus in line with the idea that 2-APB may inhibit the Ca^{2+}-dependent K^+ channels responsible for generating AHPs. Interestingly, the enhanced ADPs we observed were occasionally suprathreshold for action potential generation ($n = 3/14$ cells). Inhibition of SK channels alone is unlikely to explain the generation of these action potentials. In both layer V neocortical and hippocampal pyramidal neurons, SK channel immunoreactivity is strongest in the soma and proximal primary apical dendrites [48,49]. The smaller amplitudes and broader widths of ADP spikes suggest, however, that they were dendritically initiated. Moreover, activation of the currents underlying ADPs in pyramidal neurons requires the influx of Ca^{2+} via VGCCs. The enhanced ADPs we observe might therefore suggest an influence by 2-APB on Ca^{2+} signaling via VGCCs, a concept that is in keeping with the effects of 2-APB on SOCs [27–29,31] and TRPs [33–35]. Alternately, the larger and sometimes suprathreshold ADPs evoked in the presence of 2-APB may be secondary to the inhibition by 2-APB of dendritic voltage-dependent K^+ conductances.

The altered firing patterns and action potential waveforms we observed after adding 2-APB to our recording ACSF were accompanied by an increase in the whole-cell input resistance (11.1 ± 6.0 MΩ increase, $n = 8$; $p = 0.105$). This increase would suggest that, in addition to influencing active and/or Ca^{2+}-dependent K^+ conductances, 2-APB might also antagonize passive or leak K^+ currents. Alternately, a slight change in input resistance could simply reflect the antagonism of voltage-dependent K^+ channels that are partially activated at resting potentials (e.g., KCNQ, K_{ir}; [40]). A decrease in the resting K^+ conductance, however, would also be expected to lower the potential difference across the plasma membrane. Indeed, we found that cells were slightly more depolarized following 10–30 min bath application of 2-APB than they were in the 15 min prior to 2-APB exposure (4.6 ± 2.6 mV increase, $n = 5$; $p = 0.119$).

In order to verify that the increases in excitability we observed were specific to 2-APB exposure, and not an artifact of our recording conditions, we evaluated the progression of each measure over the course of experiments in which 2-APB was not applied. With the exception of the post-spike ADP, all measures of intrinsic excitability were relatively stable (<10% change) over time in control cells. Control ADPs, however, decreased in magnitude over time, while ADPs following 2-APB exposure were, as described above, significantly increased. In sum, we found that nearly all measured changes in excitability in cells exposed to 2-APB were significantly different from those in control cells (Table 1). Moreover, the effects of 2-APB on neuronal excitability reversed during 2-APB wash-out (Figs. 2D, E and 3B–F).

On the basis of the findings presented here, we conclude that 2-APB, in addition to inhibiting IP_3R-dependent internal Ca^{2+} release, also increases the excitability of neocortical and hippocampal and pyramidal neurons. Furthermore, we find – albeit by indirect means – that the mechanism of this increased excitability most likely involves the combined antagonism of multiple voltage-and Ca^{2+}-dependent K^+ conductances. Our findings have important implications for the interpretation of past and future studies using 2-APB to examine the consequences of IP_3R signaling. Specifically, they suggest that observed changes in cellular, network, or animal behavior following the introduction of 2-APB might not be attributable to consequently impaired IP_3R-mediated Ca^{2+} signaling, or even to changes in the activity of SOCs or SERCA pumps, but rather to unexpected or undesired changes in plasma membrane ion conductances and neuronal excitability.

We did not, in this study, evaluate the potential influence of the other membrane-permeant IP_3R antagonist, xestospongin C, on neuronal excitability. The variety of Ca^{2+}-carrying proteins and currents targeted by xestospongin C is strikingly similar to that also affected by 2-APB (IP_3Rs, SOCs, SERCA pumps). In this light, and in view of its having been reported to antagonize voltage-gated K^+ currents in smooth muscle [23], it might be sensible to test whether xestospongin C similarly alters the excitability of pyramidal neurons before turning to this drug as an alternative to 2-APB in the examination of IP_3R-mediated internal Ca^{2+} release and its consequences.

In general, the results of this study highlight the limitations of pharmacological tools employed in the study of intracellular signaling. To a certain degree, these limitations may be overcome in animal models through the use of recombinant genetic strategies such as knock-in and knock-out mice and by the use of siRNAs. The utility of genetic manipulations for the treatment of human disease, however, is very limited for the present. We therefore find that both the study of IP_3R-mediated neuronal signaling and the remediation of its dysfunction in disease would benefit highly from the development of a novel pharmacological agent specifically targeted to IP_3 receptor ion channels.

Acknowledgments

We would like to thank Len Kaczmarek for a critical reading of the manuscript, as well as Keith Gipson and Joe Santos-Sacchi for many thoughtful discussions. This work was supported by the Kavli Foundation, the Dart Foundation, NIMH RO1-MH067830 and P50-MH068789, and NIAAA 1RL1AA017536-01 (MFY), an NIH-NHLBI/Yale BioSTEP Program Fellowship (CEB), and an NSF Graduate Research Fellowship (AMH).

References

1. Berridge MJ. Neuronal calcium signaling. Neuron 1998;21:13–26. [PubMed: 9697848]
2. Kaftan EJ, Ehrlich BE, Watras J. Inositol 1,4,5-trisphosphate (InsP3) and calcium interact to increase the dynamic range of InsP3 receptor-dependent calcium signaling. J. Gen. Physiol 1997;110:529–538. [PubMed: 9348325]
3. Berridge MJ, Lipp P, Bootman MD. The versatility and universality of calcium signalling. Nat. Rev. Mol. Cell. Biol 2000;1:11–21. [PubMed: 11413485]
4. Nakamura T, Nakamura K, Lasser-Ross N, Barbara JG, Sandler VM, Ross WN. Inositol 1,4,5-trisphosphate (IP3)-mediated Ca2+ release evoked by metabotropic agonists and backpropagating action potentials in hippocampal CA1 pyramidal neurons. J. Neurosci 2000;20:8365–8376. [PubMed: 11069943]
5. Nakamura T, Lasser-Ross N, Nakamura K, Ross WN. Spatial segregation and interaction of calcium signalling mechanisms in rat hippocampal CA1 pyramidal neurons. J. Physiol 2002;543:465–480. [PubMed: 12205182]
6. Nakamura T, Barbara JG, Nakamura K, Ross WN. Synergistic release of Ca2+ from IP3-sensitive stores evoked by synaptic activation of mGluRs paired with backpropagating action potentials. Neuron 1999;24:727–737. [PubMed: 10595522]
7. Jaffe DB, Brown TH. Metabotropic glutamate receptor activation induces calcium waves within hippocampal dendrites. J. Neurophysiol 1994;72:471–474. [PubMed: 7965030]
8. Larkum ME, Watanabe S, Nakamura T, Lasser-Ross N, Ross WN. Synaptically activated Ca2+ waves in layer 2/3 and layer 5 rat neocortical pyramidal neurons. J. Physiol 2003;549:471–488. [PubMed: 12692172]
9. Power JM, Sah P. Nuclear calcium signaling evoked by cholinergic stimulation in hippocampal CA1 pyramidal neurons. J. Neurosci 2002;22:3454–3462. [PubMed: 11978822]
10. Watanabe S, Hong M, Lasser-Ross N, Ross WN. Modulation of calcium wave propagation in the dendrites and to the soma of rat hippocampal pyramidal neurons. J. Physiol 2006;575:455–468. [PubMed: 16809362]

11. Hagenston AM, Fitzpatrick JS, Yeckel MF. MGluR-mediated calcium waves that invade the soma regulate firing in layer V medial prefrontal cortical pyramidal neurons. Cereb. Cortex 2008;18:407–423. [PubMed: 17573372]
12. Gulledge AT, Kawaguchi Y. Phasic cholinergic signaling in the hippocampus: functional homology with the neocortex? Hippocampus 2007;17:327–332. [PubMed: 17407133]
13. Gulledge AT, Stuart GJ. Cholinergic inhibition of neocortical pyramidal neurons. J. Neurosci 2005;25:10308–10320. [PubMed: 16267239]
14. Stutzmann GE, LaFerla FM, Parker I. Ca2+ signaling in mouse cortical neurons studied by two-photon imaging and photoreleased inositol triphosphate. J. Neurosci 2003;23:758–765. [PubMed: 12574404]
15. Fernandez de Sevilla D, Nunez A, Borde M, Malinow R, Buno W. Cholinergic-mediated IP3-receptor activation induces long-lasting synaptic enhancement in CA1 pyramidal neurons. J. Neurosci 2008;28:1469–1478. [PubMed: 18256268]
16. Stutzmann GE, Smith I, Caccamo A, Oddo S, Laferla FM, Parker I. Enhanced ryanodine receptor recruitment contributes to Ca2+ disruptions in young, adult, and aged Alzheimer's disease mice. J. Neurosci 2006;26:5180–5189. [PubMed: 16687509]
17. Stutzmann GE. Calcium dysregulation, IP3 signaling, and Alzheimer's disease. Neuroscientist 2005;11:110–115. [PubMed: 15746379]
18. Stutzmann GE, Caccamo A, LaFerla FM, Parker I. Dysregulated IP3 signaling in cortical neurons of knock-in mice expressing an Alzheimer's-linked mutation in presenilin1 results in exaggerated Ca2+ signals and altered membrane excitability. J. Neurosci 2004;24:508–513. [PubMed: 14724250]
19. Leissring MA, Paul BA, Parker I, Cotman CW, LaFerla FM. Alzheimer's presenilin-1 mutation potentiates inositol 1,4,5-trisphosphate-mediated calcium signaling in *Xenopus oocytes*. J. Neurochem 1999;72:1061–1068. [PubMed: 10037477]
20. Gafni J, Munsch JA, Lam TH, et al. Xestospongins: potent membrane permeable blockers of the inositol 1,4,5-trisphosphate receptor. Neuron 1997;19:723–733. [PubMed: 9331361]
21. De Smet P, Parys JB, Callewaert G, et al. Xestospongin C is an equally potent inhibitor of the inositol 1,4,5-trisphosphate receptor and the endoplasmic-reticulum Ca(2+) pumps. Cell Calcium 1999;26:9–13. [PubMed: 10892566]
22. Solovyova N, Fernyhough P, Glazner G, Verkhratsky A. Xestospongin C empties the ER calcium store but does not inhibit InsP3-induced Ca2+ release in cultured dorsal root ganglia neurones. Cell Calcium 2002;32:49–52. [PubMed: 12127062]
23. Ozaki H, Hori M, Kim YS, et al. Inhibitory mechanism of xestospongin-C on contraction and ion channels in the intestinal smooth muscle. Br. J. Pharmacol 2002;137:1207–1212. [PubMed: 12466229]
24. Liu X, Ambudkar IS. Characteristics of a store-operated calcium-permeable channel: sarcoendoplasmic reticulum calcium pump function controls channel gating. J. Biol. Chem 2001;276:29891–29898. [PubMed: 11395504]
25. Castonguay A, Robitaille R. Xestospongin, C is a potent inhibitor of SERCA at a vertebrate synapse. Cell Calcium 2002;32:39–47. [PubMed: 12127061]
26. Ta TA, Feng W, Molinski TF, Pessah IN. Hydroxylated xestospongins block inositol-1,4,5-trisphosphate-induced Ca2+ release and sensitize Ca2+-induced Ca2+ release mediated by ryanodine receptors. Mol. Pharmacol 2006;69:532–538. [PubMed: 16249374]
27. Bootman MD, Collins TJ, Mackenzie L, Roderick HL, Berridge MJ, Peppiatt CM. 2-Aminoethoxydiphenyl borate (2-APB) is a reliable blocker of store-operated Ca2+ entry but an inconsistent inhibitor of InsP3-induced Ca2+ release. FASEB J 2002;16:1145–1150. [PubMed: 12153982]
28. Bilmen JG, Michelangeli F. Inhibition of the type 1 inositol 1,4,5-trisphosphate receptor by 2-aminoethoxydiphenylborate. Cell. Signal 2002;14:955–960. [PubMed: 12220621]
29. Peppiatt CM, Collins TJ, Mackenzie L, et al. 2-Aminoethoxydiphenyl borate (2-APB) antagonises inositol 1,4,5-trisphosphate-induced calcium release, inhibits calcium pumps and has a use-dependent and slowly reversible action on store-operated calcium entry channels. Cell Calcium 2003;34:97–108. [PubMed: 12767897]

30. Maruyama T, Kanaji T, Nakade S, Kanno T, Mikoshiba K. 2APB, 2-aminoethoxydiphenyl borate, a membrane-penetrable modulator of Ins(1,4,5)P3-induced Ca2+ release. J. Biochem 1997;122:498–505. [PubMed: 9348075]

31. Park MK, Lee KK, Uhm DY. Slow depletion of endoplasmic reticulum Ca2+ stores and block of store-operated Ca2+ channels by 2-aminoethoxydiphenyl borate in mouse pancreatic acinar cells. Naunyn Schmiedebergs Arch. Pharmacol 2002;365:399–405. [PubMed: 12012026]

32. Bilmen JG, Wootton LL, Godfrey RE, Smart OS, Michelangeli F. Inhibition of SERCA Ca2+ pumps by 2-aminoethoxydiphenyl borate (2-APB). 2-APB reduces both Ca2+ binding and phosphoryl transfer from ATP, by interfering with the pathway leading to the Ca2+-binding sites. Eur. J. Biochem 2002;269:3678–3687. [PubMed: 12153564]

33. Ma HT, Patterson RL, van Rossum DB, Birnbaumer L, Mikoshiba K, Gill DL. Requirement of the inositol trisphosphate receptor for activation of store-operated Ca2+ channels. Science 2000;287:1647–1651. [PubMed: 10698739]

34. Delmas P, Wanaverbecq N, Abogadie FC, Mistry M, Brown DA. Signaling microdomains define the specificity of receptor-mediated InsP(3) pathways in neurons. Neuron 2002;34:209–220. [PubMed: 11970863]

35. Hu HZ, Gu Q, Wang C, et al. 2-Aminoethoxydiphenyl borate is a common activator of TRPV1, TRPV2, and TRPV3. J. Biol. Chem 2004;279:35741–35748. [PubMed: 15194687]

36. Wang Y, Deshpande M, Payne R. 2-Aminoethoxydiphenyl borate inhibits phototransduction and blocks voltage-gated potassium channels in Limulus ventral photoreceptors. Cell Calcium 2002;32:209–216. [PubMed: 12379181]

37. Hong M, Ross WN. Priming of intracellular calcium stores in rat CA1 pyramidal neurons. J. Physiol 2007;584:75–87. [PubMed: 17690146]

38. Power JM, Sah P. Intracellular calcium store filling by an L-type calcium current in the basolateral amygdala at subthreshold membrane potentials. J. Physiol 2005;562:439–453. [PubMed: 15550460]

39. Storm JF. Potassium currents in hippocampal pyramidal cells. Prog. Brain Res 1990;83:161–187. [PubMed: 2203097]

40. Hille, B. Ion Channels of Excitable Membranes. Sunderland, Massachussetts: Sinauer Associates, Inc.; 2001. Potassium channels and chloride channels; p. 131-167.

41. Johnston, D.; Wu, MS. Foundations of Cellular Neurophysiology. Cambridge, Massachusetts: The MIT Press; 1995. Functional diversity of voltage-gated conductances; p. 183-214.

42. Kang J, Huguenard JR, Prince DA. Voltage-gated potassium channels activated during action potentials in layer V neocortical pyramidal neurons. J. Neurophysiol 2000;83:70–80. [PubMed: 10634854]

43. Abel HJ, Lee JC, Callaway JC, Foehring RC. Relationships between intracellular calcium and afterhyperpolarizations in neocortical pyramidal neurons. J. Neurophysiol 2004;91:324–335. [PubMed: 12917389]

44. Villalobos C, Shakkottai VG, Chandy KG, Michelhaugh SK, Andrade R. SKCa channels mediate the medium but not the slow calcium-activated afterhyperpolarization in cortical neurons. J. Neurosci 2004;24:3537–3542. [PubMed: 15071101]

45. Storm JF. Action potential repolarization and a fast after-hyperpolarization in rat hippocampal pyramidal cells. J. Physiol 1987;385:733–759. [PubMed: 2443676]

46. Higashi H, Tanaka E, Inokuchi H, Nishi S. Ionic mechanisms underlying the depolarizing and hyperpolarizing afterpotentials of single spike in guinea-pig cingulate cortical neurons. Neuroscience 1993;55:129–138. [PubMed: 8350984]

47. Haj-Dahmane S, Andrade R. Calcium-activated cation nonselective current contributes to the fast afterdepolarization in rat prefrontal cortex neurons. J. Neurophysiol 1997;78:1983–1989. [PubMed: 9325366]

48. Sailer CA, Hu H, Kaufmann WA, et al. Regional differences in distribution and functional expression of small-conductance Ca2+-activated K+ channels in rat brain. J. Neurosci 2002;22:9698–9707. [PubMed: 12427825]

49. Sailer CA, Kaufmann WA, Marksteiner J, Knaus HG. Comparative immunohistochemical distribution of three small-conductance Ca2+-activated potassium channel subunits, SK1, SK2, and SK3 in mouse brain. Mol. Cell. Neurosci 2004;26:458–469. [PubMed: 15234350]

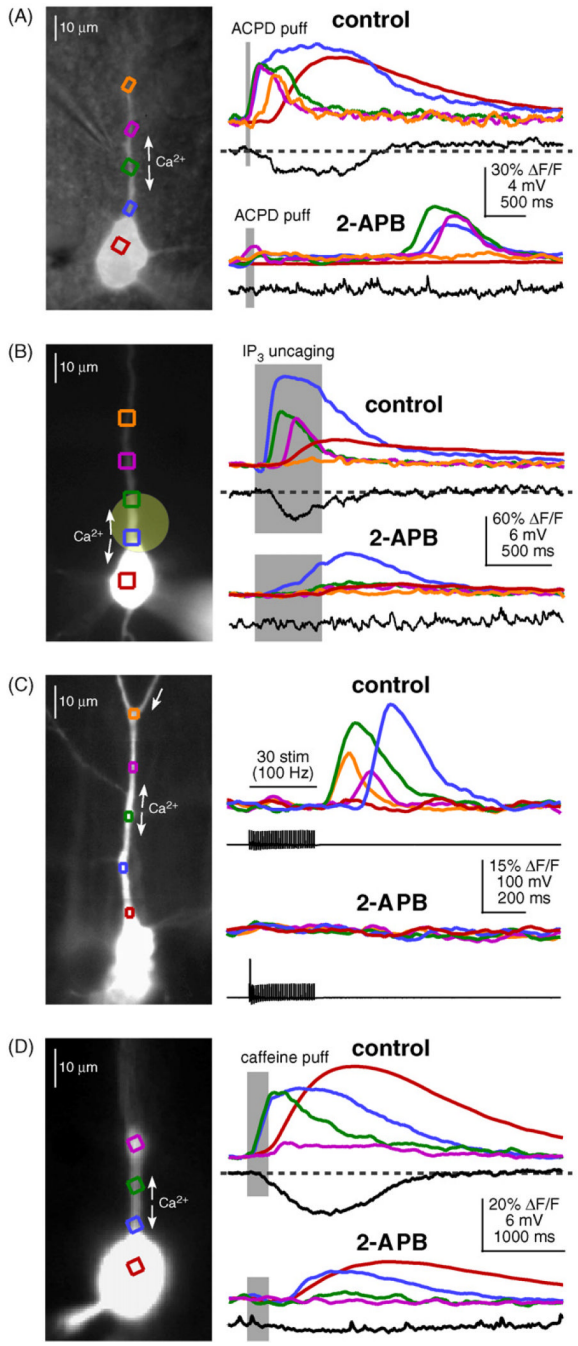

Fig. 1.

2-APB inhibited internal Ca^{2+} release in neocortical and hippocampal pyramidal neurons. (A) Left, Alexa fluorescence image of a layer V medial prefrontal cortical (mPFC) pyramidal neuron filled with bis-fura-2 (100 µM) with DIC overlay showing the approximate position of the ACPD puffer pipette. Colored boxes indicate the positions of regions of analysis corresponding to the optical traces at right. Right top, brief puffs of the group I/II mGluR agonist ACPD (400 µM, 50 ms) triggered bidirectionally propagating waves of internally released Ca^{2+} under control conditions. Note also that this Ca^{2+} wave evoked a transient hyperpolarization and prolonged depolarization [11]. Right bottom, internal Ca^{2+} release diminished in amplitude and extent after the addition of 2-APB, but was not blocked within

28 min of 2-APB exposure. Shown here is the neuron's response to a 100 ms puff of ACPD 23 min after 2-APB was added to the recording ACSF. (B) Left, fluorescence image of a layer V mPFC pyramidal neuron filled with fluo-4 (100 μM) and NPE-caged IP_3 (97 μM). The pale yellow circle shows the size (~20 μm diameter) and position of the UV uncaging beam. Right top, brief UV uncaging flashes (500 ms) consistently triggered propagating waves of internal Ca^{2+} release under control conditions. Note also that this Ca^{2+} wave evoked a transient hyperpolarization of the plasma membrane [11]. Right bottom, an IP_3-evoked Ca^{2+} signal was triggered by 500 ms flashes for the 32 min duration of 2-APB exposure. The trace shown here was recorded 32 min after 2-APB was introduced into the recording ACSF. (C) Left, Alexa fluorescence image of a CA1 hippocampal pyramidal neuron filled with fura-2ff (200 μM). Right, synaptic stimulation triggered robust propagating waves of internal Ca^{2+} release under control conditions (top), but not after 17 min treatment with bath-applied 2-APB (bottom). (D) Left, Alexa fluorescence image of a layer V mPFC pyramidal neuron filled with bis-fura-2 (100 μM). Right top, brief puffs of the ryanodine receptor agonist caffeine (50 mM, 200 ms) triggered internal Ca^{2+} release and a transient hyperpolarization under control conditions. Right bottom, the Ca^{2+} signal and the hyperpolarization were first inhibited 22 min after 2-APB was added to the recording ACSF. Shown here is the neuron's response to a 200 ms puff of caffeine 32 min after 2-APB was added to the recording ACSF. (For interpretation of the references to color in this figure legend, the reader is referred to the web version of the article.)

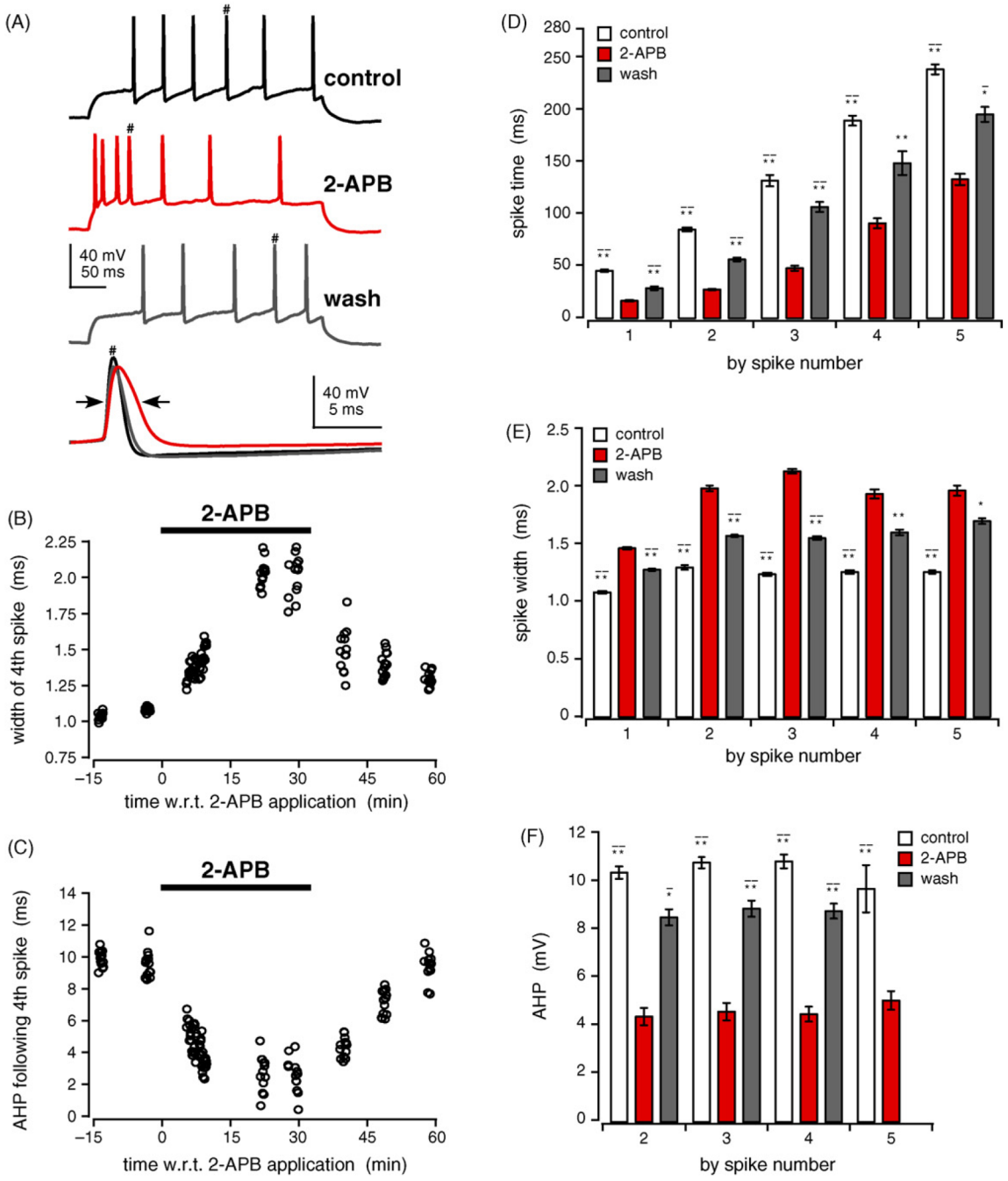

Fig. 2.

2-APB reversibly altered the firing patterns of pyramidal neurons, decreased the magnitude of AHPs, and increased the widths of action potentials. (A)–(C) A layer V mPFC pyramidal neuron was excited to fire action potentials with prolonged suprathreshold current injections (300 pA, 300 ms). (A) Example voltage responses recorded 3 min prior to 2-APB application (control), 29 min following addition of 2-APB to the recording ACSF (2-APB), and 26 min after initiation of 2-APB wash-out (wash). The fourth action potentials from example traces for each condition (indicated by # s) are overlaid using a higher temporal resolution in the bottom set of optical traces. Under control conditions and during wash-out, action potential trains were evoked after a delay. The length of this delay decreased and the initial rate of action

potential firing increased in the presence of 2-APB. The width of action potentials at half-maximum was noticeably greater during 2-APB application than under control conditions or following 2-APB wash-out (arrows). Action potentials evoked under control conditions exhibited robust AHPs. These AHPs were diminished during 2-APB exposure, but increased in amplitude again during the drug wash-out. (B) The widths of the fourth action potentials evoked by prolonged current injections are plotted as a function of time. Spike width increased during 2-APB exposure, and decreased as 2-APB was washed out. (C) The magnitudes of AHPs following the fourth action potentials evoked by prolonged current injections are plotted as a function of time. AHP magnitudes dropped sharply after 2-APB application, but exhibited recovery during wash-out. (D) The mean amounts of time between the start of depolarizing current injection and the peak of each action potential in a train are displayed for recordings made in the 15 min prior to 2-APB application (control; $n = 12$), between 10 and 30 min after 2-APB was added to the recording media (2-APB; $n = 12$), and at the end of the wash-out period between 15 and 30 min following the switch from 2-APB to control recording media (wash; $n = 6$). Action potentials evoked in the presence of 2-APB were triggered significantly earlier than action potentials evoked under control conditions or during 2-APB wash-out. (E) Left, normalized spike widths relative to control (100%) of the first through fifth spikes evoked by prolonged current injections. Right, plotted are the mean spike widths for all spikes evoked under control ($n = 12$), 2-APB ($n = 12$), and wash conditions ($n = 6$). The widths of action potentials in the presence of 2-APB were significantly greater than those observed under control or wash conditions. (F) Left, normalized AHP magnitudes relative to control (100%) for the second through fifth spikes evoked by prolonged current injections. Right, plotted are the mean AHPs for all spikes evoked under control ($n = 11$), 2-APB ($n = 11$), and wash conditions ($n = 5$). The amplitudes of AHPs in the presence of 2-APB were significantly smaller than those observed under control or wash conditions. Statistical significance relative to measures obtained during 2-APB exposure was determined using two-tailed unpaired Student's *t*-tests (*$p < 0.05$; **$p < 0.01$; *¯$p < 0.005$; *¯*¯ $p < 0.001$).

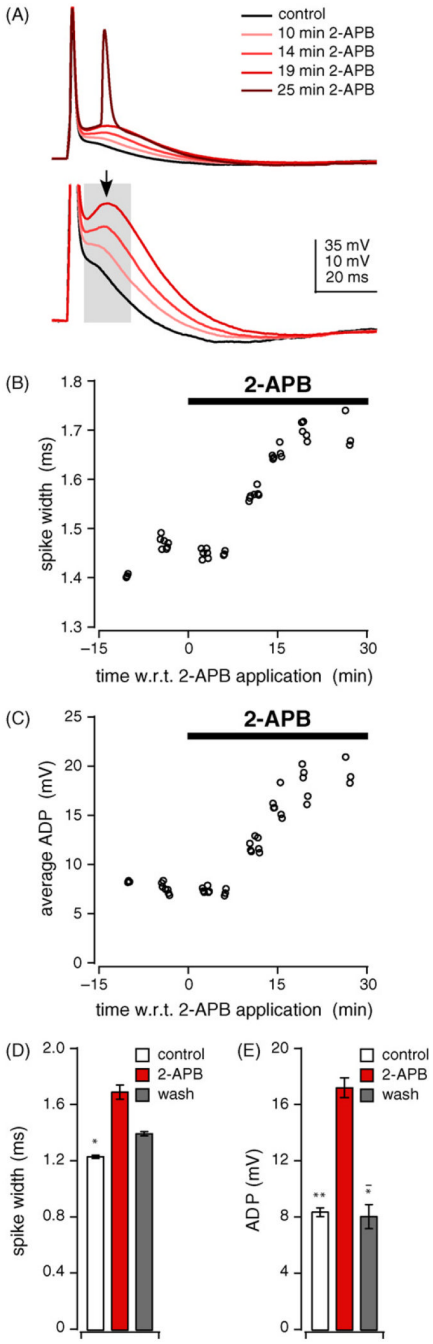

Fig. 3.

Pyramidal neurons exhibited pronounced post-spike ADPs in the presence of 2-APB. (A)–(C) Action potentials were evoked with 2500 pA, 2 ms suprathreshold current injections in a layer V mPFC pyramidal neuron under control conditions and during wash-in of 2-APB. (A) Example voltage responses illustrating the amplitude of the post-spike ADP during 2-APB wash-in. Near the end of the wash-in (25 min), the amplitude of the ADP was suprathreshold for action potential generation. The pale grey bar indicates the time period over which the average post-spike ADP illustrated in B was calculated. (B) The average amplitude of the post-spike ADP is plotted as a function of time. ADP amplitude increased sharply following addition of 2-APB to the recording ACSF. (C) Plotted as a function of time is the full width of action

potentials at half their maximum amplitude. Spike widths increased markedly following 2-APB application. (D) Mean ADP magnitudes for spikes evoked with 2 ms suprathreshold current injections in the 15 min prior to 2-APB application (control; $n = 13$), between 10 and 30 min after 2-APB was added to the recording media (2-APB; $n = 13$), and between 15 and 30 min following the switch from 2-APB back to control recording media (wash; $n = 3$). ADPs evoked following bath application of 2-APB were significantly greater than those evoked under control or wash conditions. (E) Mean widths of action potentials evoked with 2 ms suprathreshold current injections under control ($n = 14$), 2-APB ($n = 14$), and wash conditions ($n = 3$). The widths of spikes evoked during 2-APB exposure were significantly greater than those for spikes evoked under control or wash conditions. Statistical significance relative to measures obtained during 2-APB exposure was determined using two-tailed unpaired Student's *t*-tests (*$p < 0.05$; **$p < 0.01$; *¯$p < 0.005$).

Table 1

Summary of the changes in measures of intrinsic excitability observed in control pyramidal neurons and in pyramidal neurons treated with 2-APB.

Measurement	Control neurons			Neurons treated with 2-APB		
	"Drug"–"control" (given units)	**"Drug"/"control" (%)**	***N***	**Drug–control (given units)**	**Drug/control (%)**	***N***
Resting membrane potential	1.7 ± 3.5 mV	103.0 ± 6	4	−4.6 ± 2.6 mV	92.3 ± 4.6	5
Input resistance	−5.3 ± 4.7 MΩ	94.0 ± 5.5	5	11.1 ± 6.0 MΩ	113.0 ± 6.3**	8
Time of the 1st spike	1.8 ± 3.3 ms	108.6 ± 14.9	5	−29.8 ± 3.6 ms	36.5 ± 9.2***	12
Frequency of spikes in the 1st 100 ms	−2.8 ± 0.2 Hz	88 .0 ± 9.6	5	13.4 ± 0.4 Hz	151.0 ± 11.3***	11
Mean AHP (spikes 2–4)	0.35 ± 0.8 mV	103.5 ± 7.6	5	−6.1 ± 0.9 mV	42.0 ± 17.9*	11
Mean spike width (spikes 2–4)	−0.10 ± 0.06 ms	92.5 ± 4.4	5	0.75 ± 0.07 ms	159.6 ± 4.3***	12
ADP	−3.5 ± 1.3 mV	66.0 ± 13.9	7	8.8 ± 1.9 mV	204.8 ± 13.6***	13
Spike width	0.01 ± 0.04 ms	101.0 ± 3.6	7	0.45 ± 0.14 ms	136.7 ± 8.5***	14

Measures of intrinsic excitability in control neurons and in neurons treated with 2-APB were measured over the course of experiments. Mean values for "control" and "drug" conditions in control neurons were calculated from measurements taken 0–15min and 30–45 min, respectively after initial assessments of neuron health and electrical stability were completed. Mean values for control and drug conditions in neurons treated with 2-APB were measured in the 15 min prior to, and 10–30 min following 2-APB application, respectively. Values given reflect either differences between the means of these measures ("drug"–"control"; drug–control) or the ratio of these measures ("drug"/"control"; drug/control).

* Statistical significance relative to control neurons ($p < 0.05$).

** Statistical significance relative to control neurons ($p < 0.005$).

*** Statistical significance relative to control neurons ($p < 0.001$).